Published in final edited form as:
Arthritis Rheum. 2008 July ; 58(7): 2019–2029. doi:10.1002/art.23546.

Elucidating Bone Marrow Edema and Myelopoiesis in Murine Arthritis Using Contrast-Enhanced Magnetic Resonance Imaging

Steven T. Proulx[1], **Edmund Kwok**[1], **Zhigang You**[1], **M. Owen Papuga**[1], **Christopher A. Beck**[1], **David J. Shealy**[2], **Laura M. Calvi**[1], **Christopher T. Ritchlin**[1], **Hani A. Awad**[1], **Brendan F. Boyce**[1], **Lianping Xing**[1], and **Edward M. Schwarz**[1]

1*Steven T. Proulx, PhD, Edmund Kwok, PhD, Zhigang You, MS, M. Owen Papuga, MS, Christopher A. Beck, PhD, Laura M. Calvi, MD, Christopher T. Ritchlin, MD, Hani A. Awad, PhD, Brendan F. Boyce, MBChB, Lianping Xing, PhD, Edward M. Schwarz, PhD: University of Rochester, Rochester, New York*

2*David J. Shealy, PhD: Centocor Research and Development, Radnor, Pennsylvania*

Abstract

Objective—While bone marrow edema (BME) detected by magnetic resonance imaging (MRI) is a biomarker of arthritis, its nature remains poorly understood due to the limitations of clinical studies. In this study, MRI of murine arthritis was used to elucidate its cellular composition and vascular involvement.

Methods—BME was quantified using normalized bone marrow intensity (NBMI) from precontrast MRI and normalized marrow contrast enhancement (NMCE) following intravenous administration of gadopentate dimeglumine. Wild-type (WT) and tumor necrosis factor (TNF)-transgenic mice were scanned from 2 to 5 months of age, followed by histologic or fluorescence-activated cell sorting (FACS) analysis of marrow. In efficacy studies, TNF-transgenic mice were treated with anti-TNF or placebo for 8 weeks, and then were studied using bimonthly MRI and histologic analysis.

Results—NBMI values were similar in WT and TNF-transgenic mice at 2 months. The values in WT mice steadily decreased thereafter, with mean values becoming significantly different from those of TNF-transgenic mice at 3.5 months (mean ± SD 0.29 ± 0.08 versus 0.46 ± 0.13; $P < 0.05$). Red to yellow marrow transformation occurred in WT but not TNF-transgenic mice, as observed histologically at 5 months. The marrow of TNF-transgenic mice that received anti-TNF therapy converted to yellow marrow, with lower NBMI values versus placebo at 6 weeks (mean ± SD 0.26 ± 0.07 versus 0.61 ± 0.22; $P < 0.05$). FACS analysis of bone marrow revealed a significant correlation between NBMI values and CD11b+ monocytes ($R^2 = 0.91$, $P = 0.0028$). Thresholds for “normal”

Address correspondence and reprint requests to Edward M. Schwarz, PhD, Center for Musculoskeletal Research, University of Rochester Medical Center, 601 Elmwood Avenue, Box 665, Rochester, NY 14642. E-mail: Edward_Schwarz@URMC.Rochester.edu..

Dr. Shealy owns stock and stock options in Johnson & Johnson. Dr. Ritchlin has received consulting fees, speaking fees, and/or honoraria (less than $10,000 each) from Wyeth, Amgen, Abbott, Centocor, Bristol-Myers Squibb, and Roche. Dr. Schwarz has received consulting fees, speaking fees, and/or honoraria (less than $10,000 each) from Amgen, Centocor, and Abbott; he owns stock or stock options in Amgen and LAGeT. Dr. Schwarz has provided expert testimony on inflammatory bone loss for Amgen. He also has received research grants from Amgen and Centocor.

AUTHOR CONTRIBUTIONS

Drs. Schwarz and Proulx had full access to all of the data in the study and take responsibility for the integrity of the data and the accuracy of the data analysis.

Study design. Schwarz, Kwok, You, Shealy, Calvi, Ritchlin, Awad, Boyce, Xing, Proulx.
Acquisition of data. Kwok, You, Awad, Proulx.
Analysis and interpretation of data. Schwarz, Kwok, Beck, Shealy, Calvi, Ritchlin, Awad, Boyce, Xing, Papuga, Proulx.
Manuscript preparation. Schwarz, Kwok, You, Beck, Shealy, Calvi, Ritchlin, Awad, Boyce, Xing, Papuga, Proulx.
Statistical analysis. Schwarz, Beck, Proulx.
Provision of reagents. Shealy.

red marrow versus pathologic BME were established, and it was also found that inflammatory marrow is highly permeable to contrast agent.

Conclusion—BME signals in TNF-transgenic mice are caused by yellow to red marrow conversion, with increased myelopoiesis and increased marrow permeability. The factors that mediate these changes warrant further investigation.

Inflammatory erosive arthropathies, including rheumatoid arthritis (RA) and psoriatic arthritis, are common joint disorders that affect >1% of the population (1,2). The important role of inflammatory cytokines, particularly tumor necrosis factor (TNF), in the pathogenesis of synovial inflammation and joint destruction has been firmly established, and TNF antagonism is regarded as a therapeutic breakthrough for patients with these disorders (3). Despite these clinical advances, several pivotal questions related to the biology of inflammatory erosive arthritis have not been addressed. Of particular importance is the need to identify biomarkers of early disease before irreversible joint damage has occurred.

Active research is focused on bone marrow edema (BME), an enigmatic signal that appears on magnetic resonance imaging (MRI) scans of patients with arthritis (4-6). BME is a term with broad meaning that is audience dependent. BME in the wrist has been shown to be a predictor of eventual bone erosions at the same site (7-9), and BME may be a better indicator of joint damage than MRI-detected synovitis or traditional clinical outcome measures (10). Studies have also shown a correlation between BME and pain (11,12). Perhaps the most advanced use of this biomarker is in the evaluation of patients with ankylosing spondylitis, where an anti-TNF therapy-induced reduction in BME signals has been correlated with amelioration of disease and a patient's ability to return to work (13,14).

Despite increased attention, little has been published on the histologic correlates of BME. This is largely due to the difficulty in procuring bone biopsy specimens of BME lesions from patients with arthritis. Recent histologic studies of tissue retrieved at joint replacement surgery correlated a cellular infiltrate in close proximity to a cortical break with radiologically identified BME (6,15-17). Immunohistochemical analysis determined that B cells were the predominant cells in the affected marrow (18). However, it has not been possible to perform similar analyses on bone from patients with early arthritis, making natural history studies impossible. Therefore, novel imaging methods using animal models are needed to characterize BME in early arthritis and to define its role in the pathogenesis of synovitis and focal erosion.

To elucidate the nature of BME, we have developed high-resolution MRI to visualize and quantify in vivo biomarkers in mice with knee arthritis (19,20). During the course of our investigations, we noticed 2 distinct patterns of enhanced signal in the bones of TNF-transgenic mice versus their wild-type (WT) littermates. One pattern appeared as a bright contrastenhancing signal in the subchondral regions of inflamed joints, similar to BME as described in the clinical literature (7-9), while the other presented as a diffuse signal throughout the bone marrow. This second signal was observed early in the disease process before focal erosions could be detected by microfocal computed tomography (micro-CT). The current study was undertaken to evaluate this BME pattern in more detail and to better understand the contribution of specific cell types to events in the subchondral bone marrow. We also investigated the relationship between TNF-induced BME and the increased myelopoiesis responsible for the generation of CD11b+ osteoclast precursors in mice (21-24) and in patients with inflammatory erosive arthritis (25).

MATERIALS AND METHODS

Animals and anti-TNF treatment

The 3647 line of TNF-transgenic mice, which develops inflammation and erosive arthritis much later than the 197 line (26), was obtained from Dr. George Kollias (Institute of Immunology, Alexander Fleming Biomedical Sciences Research Center, Vari, Greece), and the mice were maintained as heterozygotes in a CBA × C57BL/6 background (27). Experiments were performed with sex-matched TNF-transgenic mice and WT littermate controls under protocols approved by the Institutional Animal Care and Use Committee.

An initial natural history study of marrow edema was performed, as previously described (20). TNF-transgenic and WT mice (n = 5 per group) underwent MRI beginning at 2 months of age, and were scanned bimonthly until they were 5 months of age. We were unable to collect data at 4 months of age due to temporary technical problems with the scanner.

In drug intervention studies, mice received either murine monoclonal anti-TNF anti-human IgG1 antibody or an irrelevant murine IgG1 placebo control (Centocor R&D, Radnor, PA) at a dosage of 10 mg/kg/week intraperitoneally, as previously described (28). We studied 2 groups of mice, each with 4 female TNF-transgenic animals. These mice were scanned every 2 weeks starting at 3 months of age and were entered into the study when their synovial volumes, as detected by contrast-enhanced MRI, rose above 3 mm^3. The mean ± SD age of mice at initiation of treatment was 3.9 ± 0.8 months. One group received weekly anti-TNF injections, while the second group received placebo. MRI scans were performed at baseline and every 2 weeks for 8 weeks. At 8 weeks, mice were killed and the knee and ankle joints were harvested for histologic analysis.

Magnetic resonance imaging

Images were obtained using a Trio 3.0T scanner (Siemens, Erlangen, Germany), as previously described (20). Briefly, mice were anesthetized and positioned on an imaging platform for localization scans, followed by a fat-suppressed, high-resolution scan (sagittal 3-dimensional fast low-angle shot [FLASH]). The acquisition parameters were as follows: flip angle 25°, repetition time (TR) 45 msec, echo time (TE) 9.03 msec, matrix 192 × 192 pixels, field of view 20 × 20 mm, slice thickness 0.16 mm, acquisition time 8 minutes, 28 seconds, and 1 acquisition. For this gradient-echo sequence, the short TR and TE values gave this sequence T1-weighting, while the low flip angle value gave T2-weighting. Gadopentate dimeglumine (Gd-DTPA) (Omniscan; Amersham Health, Oslo, Norway), at a dose of 0.5 ml/kg and diluted in sterile saline, was injected via the retroorbital venous plexus. After 3 minutes, a second high-resolution scan was performed with contrast enhancement. Imaging sessions took ~30 minutes per mouse.

MRI data analysis

An OsiriX DICOM viewer was used for image processing and analysis. To perform quantitative longitudinal assessments of MRI signal intensities, a method was developed to normalize for signal variations that are present between scans due to differences in mouse positioning in the knee coil or fluctuations in field strength. Region of interest (ROI) circles (~0.7 mm^2) were drawn on 5 contiguous 2-dimensional slices in the tibial marrow at a distance of 1 mm from the proximal end of the tibial plateau. The ROI was copied and placed in the gastrocnemius muscle at an equivalent distance from the center of the coil. The muscle serves as a normalization tissue, since its MRI signal with and without contrast is not affected by joint inflammation. The average value of mean marrow signal intensity divided by mean muscle signal intensity for 5 slices is known as normalized bone marrow intensity (NBMI).

On postcontrast scans the ROIs in the tibial marrow were copied from the precontrast scans. The average value of the mean signal intensity of the ROIs on the postcontrast scans is known as marrow contrast enhancement. This value is typically normalized for dosage variations by dividing by the contrast enhancement value of a large 3-dimensional section of muscle (>15 mm^3), segmented and analyzed using Amira 3.1 software (Mercury Computer Systems, Chelmsford, MA), as previously described (20). The normalized value is termed normalized marrow contrast enhancement (NMCE). Analysis of both quantifications takes ~15 minutes by an experienced operator.

Reproducibility of BME measurements was assessed for intrareader, interreader, and inter-MRI variation. For intrareader variation, 10 contrast-enhanced MRI scans (5 TNF-transgenic and 5 WT mice) were analyzed by the same operator (STP) on 2 different days in random order. A second operator (MOP) analyzed the same 10 scans after a training period of 1 hour to determine interreader variation. For inter-MRI variation, 8 TNF-transgenic mice with BME of varying severity were scanned twice within 48 hours and the same operator analyzed the scans in random order.

Histologic examination

The right knee and ankle joints were removed and fixed in 10% neutral buffered formalin. The joints were decalcified in 14% EDTA at room temperature (pH adjusted to 7.2) for 21 days. Joints were then carefully embedded in paraffin for sectioning into 3-μm slices. Sections were stained with hematoxylin and eosin, Alcian blue, and orange G for histologic examination, as previously described (29).

Immunohistochemical analysis to identify T cells, B cells, macrophages, and neutrophils was performed, as previously described (18), using primary antibodies specific for CD3 (1:100; Novocastra, Newcastle, UK), CD45R/B220 (1:300; BD PharMingen, San Diego, CA), F4/80 (1:80; Serotec, Raleigh, NC), and Neu7/4 (clone MCA771G, 1:2,000; Serotec), respectively.

Histomorphometry

Knee joint sections containing the tibial middiaphyseal red marrow were used for histomorphometric analysis of marrow vascularity by the point-counting steriometric method, as previously described (30). Sections from WT and TNF-transgenic mice treated with placebo or anti-TNF for 8 weeks (n = 3 per group) were used for analysis. For each mouse, 3 different levels comprising tibial marrow were analyzed. On each level, 3 regions (each 0.04 mm^2) of marrow consisting of purely cellular regions without adipocytes were analyzed at a distance of ~5 mm from the proximal growth plate using point counting. Vascular regions (defined as dense accumulations of red blood cells) versus hematopoietic regions were counted. The proportion of vascular regions divided by total area analyzed is defined as the vascular area (mm^2 per mm^2 of red marrow).

Fluorescence-activated cell sorting (FACS) analysis

Five-month-old TNF-transgenic and WT mice (n = 3 per group) were killed and tibial marrow was harvested for FACS analysis, as previously described (21). Cells were then labeled with fluorescence probes: allophycocyanin-anti-murine CD11b (BD PharMingen), fluorescein isothiocyanate (FITC)-anti-murine Ly-6G and Ly-6C (Gr-1) (BD PharMingen), FITC-anti-murine CD3 (Serotec), or FITC-anti-murine CD45R/B220 (BD PharMingen). Data were acquired with a FACS-Calibur instrument (BD Biosciences, Bedford, MA) and analyzed using WinMDI software (Scripps Research Institute, La Jolla, CA).

Statistical analysis

Linear mixed-effects regression models, with mouse as a random effect and time (treated as a continuous covariate) as a fixed effect, were used to assess changes over time based on longitudinal data. Similar models used age instead of time to assess changes with respect to age based on repeated measurements. Analyses based on cross-sectional data used standard linear regression models. Two-sided *t*-tests assuming unequal variances were used to make comparisons of histomorphometry, or contrast-enhanced MRI data between groups at the same time point or age.

Correlations between measures were estimated using Pearson's correlation coefficient and tested for significance using a 2-sided *t*-test. Interreader, intrareader, and inter-MRI reliability was estimated using intraclass correlation coefficients (ICCs) based on random-effects analysis of variance models. All underlying assumptions of the parametric methods were checked, and no serious violations were detected. *P* values less than 0.05 were considered significant, and *P* values less than 0.01 were considered highly significant.

RESULTS

MRI biomarkers of BME

With the aid of a custom surface coil and carefully designed MRI pulse sequence, we were able to generate images that could clearly differentiate the marrow of TNF-transgenic and WT mice on both precontrast and postcontrast scans (Figure 1). Of particular interest was the hyperintense marrow of TNF-transgenic mice on precontrast scans (NBMI = 0.59) (Figure 1A) that was markedly brighter after contrast enhancement (NMCE = 1.02) (Figure 1B), suggestive of highly vascular and/or permeable tissue (31). Corresponding histologic analysis of this region (Figure 1C) demonstrated the presence of highly cellular hematopoietic tissue throughout the marrow cavity. In contrast, the bone marrow of 5-month-old WT mice was dark in both precontrast (NBMI = 0.16) (Figure 1D) and postcontrast (NMCE = 0.34) (Figure 1E) sequences, and the corresponding histologic examination (Figure 1F) showed that the tibial metaphyseal region contained a high percentage of adipocytes, indicating a predominantly yellow marrow phenotype. The hypointensity in the metaphyseal region of WT mice is partly due to fat suppression, which was incorporated into the MRI pulse sequence.

Intrareader, interreader, and inter-MRI reliability of marrow MRI biomarkers was measured using ICC analysis, and was found to be excellent for all variables. NBMI was found to have ICC values of 0.998 for intrareader, 0.997 for interreader, and 0.982 for inter-MRI reliability. NMCE quantifications had ICC values of 0.981, 0.984, and 0.944, respectively.

Conversion of red marrow to yellow marrow in aging WT mice, but not in TNF-transgenic mice

The yellow marrow pattern seen in 5-month-old WT mice led us to hypothesize that MRI could track the conversion from cellular, red marrow to fatty, yellow marrow, which is a natural consequence of aging in the bones of mammals (32). To test this hypothesis in a natural history study, 5 WT and 5 TNF-transgenic animals received bimonthly MRI scans from 2 to 5 months of age. Quantification (Figure 1G) showed a significant decrease in NBMI with increasing age in WT animals (slope = -0.084, $P < 0.0001$) as red marrow was converted to fat (Figure 1F). TNF-transgenic animals, in contrast, showed a highly significant increase in this value from 2 to 5 months (slope = 0.040, $P < 0.0001$). In addition, NMCE (Figure 1H) showed a highly significant decrease in WT mice (slope = -0.201, $P < 0.0001$), whereas TNF-transgenic mice had a significant increase in this value (slope = 0.065, $P < 0.05$). These results indicate that the diminishing signals in WT mice are associated with red to yellow marrow conversion, while

the elevated bone marrow signal persists in TNF-transgenic mice because they do not undergo marrow conversion.

Conversion of red marrow to yellow marrow in TNF-transgenic animals following anti-TNF therapy

To further validate our marrow quantifications, and to determine if yellow marrow conversion could be induced in TNF-transgenic animals, we tested the hypothesis that anti-TNF therapy administered to TNF-transgenic mice would significantly lessen both the NBMI and the NMCE. We observed a decrease in signal intensity in the marrow from baseline (Figure 2A) to 8 weeks after the initiation of therapy (Figure 2B) in 3-month-old TNF-transgenic mice that received anti-TNF therapy. The corresponding histologic analysis (Figure 2C) revealed a high proportion of adipocytes in the bone marrow. In contrast, there was an increase in signal intensity in the marrow of placebo-treated TNF-transgenic mice from baseline (Figure 2D) to 8 weeks (Figure 2E), characterized by highly cellular marrow throughout the bones (Figure 2F). Mean NBMI (Figure 2G) and NMCE (Figure 2H) values changed significantly over time. In mice receiving anti-TNF therapy, NBMI and NMCE values decreased significantly during the 8 weeks of treatment (slopes = -0.044, $P < 0.0001$ and -0.081, $P < 0.0001$, respectively). Mean NBMI values increased significantly in placebo-treated animals (slope = 0.011, $P < 0.05$), while mean NMCE remained elevated but did not change. A highly significant treatment effect (difference in slopes between placebo and anti-TNF therapy) was found for both NBMI (0.055, $P < 0.0001$) and NMCE (0.094, $P < 0.0001$). These results show that TNF is responsible for the persistence of red marrow in TNF-transgenic mice, because inhibition of this cytokine resulted in red to yellow marrow conversion.

Effect of joint synovitis on diffuse bone marrow patterns in adjacent marrow

Results of histologic examinations of 5-month-old TNF-transgenic mice and their WT littermates were compared, to better understand the origin of marrow conversion in our model. We also wanted to determine if the hypercellular marrow pattern was generated in response to signals derived from the adjacent inflamed joint, or if it resulted from endocrine effects due to elevated levels of TNF in the systemic circulation of TNF-transgenic mice. The histologic analysis showed that in WT mice, marrow of the distal lower limb at 5 months of age was entirely filled with adipose tissue (Figure 3A). Interestingly, the marrow in the distal tibiae of their TNF-transgenic littermates was also filled with fat, despite very severe ankle arthritis, as demonstrated by the presence of cortical breaks and synovial infiltration from the adjacent joint (Figure 3B). This suggests that local joint inflammation is not responsible for the induction of marrow conversion, even when it is in direct contact with yellow marrow through infiltrating pannus tissue.

We observed a different pattern of marrow cellularity in the proximal tibiae of TNF-transgenic mice, in which the histologic analysis showed hypercellular marrow irrespective of the severity of knee inflammation. As an example, Figure 3C shows the knee histology in a TNF-transgenic mouse with little to no joint inflammation (Figure 3E) but predominantly red marrow (Figure 3G) and elevated signals on MRI (NBMI = 0.587). In contrast, Figure 3D shows the histology in a TNF-transgenic mouse with severe arthritis (Figure 3F), which also exhibited hypercellular marrow (NBMI = 0.688) (Figure 3H). Collectively, these findings indicate that the increases in cellular marrow in TNF-transgenic animals follow a distinct pattern from central to distal joints, which is a reverse pattern from the yellow marrow conversion that takes place in growing individuals (32).

Marrow conversions and their relationship to vascularity

The tibial diaphyses of 5-month-old TNF-transgenic mice show the region in which systemic marrow conversions occurred. Histologic examination of TNF-transgenic mice (Figures 3I and

J) revealed the marrow conversion front as a highly vascularized region that contains large numbers of erythrocytes in expanded vascular channels between the monocytes and fat. In contrast, the marrow conversion front in TNF-transgenic mice treated with anti-TNF for 8 weeks (Figures 3K and L) was characterized by tissue containing few erythrocytes. To demonstrate the significance of this vascularity, we performed histomorphometry to quantify these erythrocytic regions within the red marrow of the middiaphysis in the tibiae of WT, TNF-transgenic, and anti-TNF-treated TNF-transgenic mice (Figure 3M). We determined that TNF-transgenic mice had a highly significant increase in these vascular areas of red marrow compared with WT animals. Furthermore, anti-TNF therapy significantly reduced these vascular areas in TNF-transgenic mice to levels observed in WT mice. Thus, our interpretation of these results is that TNF prevents conversion of red to yellow marrow along a proximal to distal axis, while loss of vascularity is associated with conversion to yellow marrow in response to effective anti-TNF therapy.

Diffuse BME signals are associated with increased myelopoiesis, while focal edema signals colocalize with invading pannus through cortical breaks

To further define the nature of the persisting red marrow in TNF-transgenic mice, we performed FACS analyses of marrow-derived cells from the tibiae of 5-month-old WT and TNF-transgenic mice (Figures 4A-D). While we failed to detect any significant differences in lymphocyte populations, FACS analysis revealed a dramatic increase in the percentage of CD11b+,Gr-1+ myeloid cells in the marrow of TNF-transgenic mice and most of these were in the CD11b+,Gr-1^{low} population, which consists mostly of dividing myeloid precursors, as previously described (22). To assess a potential direct relationship between elevated MRI signals and myelopoiesis, we compared the percentage of CD11b+ cells in the tibia versus the NBMI of the tibia from MRI analysis using linear regression analysis, and found a highly significant correlation ($R^2 = 0.914$, $P = 0.0028$). This supports the conclusion that diffuse, generalized BME signals can partly be caused by TNF-induced myelopoiesis.

Furthermore, TNF-transgenic mice >8 months old typically have severe erosive arthritis that leads to cortical breaks and contiguous pannus that spans from the synovial lining of the knee joint into the bone marrow (27). Interestingly, in addition to the diffuse BME signal throughout their distal femora and proximal tibiae, these mice have higher signal intensity in the marrow adjacent to the synovium (Figure 4E), which showed greater marrow contrast enhancement compared with the diffuse BME postcontrast (Figure 4F). Corresponding histologic analysis of this focal BME pattern (Figure 4G) confirmed pannus invasion of the marrow space through a cortical break in the femur. Immunohistochemical analysis of F4/80+ cells (Figure 4H) demonstrated that the infiltrating cells in mice with subchondral BME were predominantly monocyte/macrophages, which is consistent with the FACS data.

BME in TNF-transgenic mice is associated with increased Gd-DTPA perfusion

Although the aforementioned results suggest that the elevated marrow signals are associated with red marrow myelopoiesis, we also made several observations that clearly indicated that further abnormalities in red marrow must occur in order to present as BME on MRI. First, the MRI signal in older WT animals with incomplete marrow conversion appeared dark in both the red and the yellow marrow regions of the tibia (Figures 1D-F). Second, the vascular area was increased in TNF-transgenic mice over WT mice in these persisting red marrow areas (Figure 3M). Third, there was a dramatic difference in the contrast-enhancement patterns of the tibial diaphysis between WT and TNF-transgenic mice at 5 months of age (Figure 5). In WT mice at this age, red marrow persisted in the diaphysis of the marrow (Figure 5A) and was supplied with blood by the large nutrient artery (Figure 5B). This artery was clearly visualized on precontrast and postcontrast MRIs (Figures 5C and D). However, there was no corresponding edema signal or contrast enhancement in the red marrow surrounding this artery.

In contrast, in TNF-transgenic animals, the nutrient artery was seen on histologic examination (Figures 5E and F), but could not be visualized on MRIs (Figures 5G and H) due to high signal intensity throughout the marrow. These results suggest that the vascular endothelium in the marrow of TNF-transgenic mice is highly permeable, which causes increased NBMI due to excess interstitial fluid and increased NMCE due to diffusion of the Gd-DTPA throughout the marrow space.

MRI thresholds of yellow marrow, normal red marrow, and BME

Given that there is a broad spectrum of signals from normal and pathologic red marrow, we performed a linear regression analysis of the NBMI versus NMCE signals from the WT and TNF-transgenic mice shown in Figure 1 and from the anti-TNF-treated mice shown in Figure 2 (Figure 6). This analysis demonstrated a highly significant correlation ($R^2 = 0.812$, $P < 0.0001$) between NBMI and NMCE in all of the tibiae examined. Moreover, we were able to identify apparent thresholds that defined the yellow versus normal red marrow versus pathologic red marrow that presents as BME.

DISCUSSION

Despite the increasing usage of BME as a clinical biomarker of arthritis, the cellular and molecular constituents that give rise to BME signals remain very poorly understood (4). To elucidate the nature of these BME signals, we performed a systematic quantitative contrast-enhanced MRI and histologic evaluation of the knee joints of WT and TNF-transgenic mice. We discovered a diffuse BME pattern in arthritic mice, distinct from subchondral BME that coexists with focal erosions. This persistent inflammatory red marrow was associated with increased myelopoiesis and increased perfusion of Gd-DTPA contrast agent. Amelioration of this marrow pattern was seen after effective anti-TNF therapy, highlighting the role of long-term TNF treatment in this process.

Clinical recommendations for MRI examination of BME suggest a T2-weighted sequence or a T1-weighted sequence with Gd-DTPA to visualize edema as a hyperintense region of the marrow (33). Typically, T1-weighted sequences show increased water content as low intensity. However, the 3-dimensional FLASH shot used in the current study is able to visualize edema as “bright” on scans both before and after administration of Gd-DTPA. This is due to both T1- and T2-weighted characteristics being built into the FLASH sequence. This “dual-weighting” facilitated quantification of BME by allowing image subtraction of precontrast scans from postcontrast scans. Unlike dynamic contrast-enhanced MRI methods that have recently been applied to BME (34), which use time as a denominator for quantification of enhancement, the current method uses surrounding muscle as a normalization tissue. This allowed normalization of quantifications of both precontrast (NBMI) and postcontrast (NMCE) scans to be developed and validated. Although reproducibility studies demonstrated that NBMI was the more reliable measure, NMCE may have the advantage of increased sensitivity, as shown by the larger treatment effect values after anti-TNF therapy.

Although the generalized pattern of marrow conversion to inflammatory red marrow from central to distal joints in TNF-transgenic mice has not been described in RA, it is possible that it has been overlooked. Typically, BME in RA is seen on MRIs of affected distal joints such as the wrist (8). This subchondral BME is described in close conjunction with focal erosions, and may be a “reaction” of the bone marrow to infiltrating synovium (18). However, in our TNF-transgenic mouse model we did not see evidence of subchondral bone marrow changes until late in the disease process. Systemic marrow conversions of the type shown here would likely be initiated at central joints that would not be assessed in RA. However, marrow biopsies of red marrow locations, such as the iliac crest, in adults with RA showed abnormal marrow that was due to elevated TNF levels (35). In addition, marrow from RA patients has shown an

increased percentage of myeloprogenitor cells, similar to our findings in TNF-transgenic mice (36,37). A histologic study of resected knee and hip joints revealed increased red marrow in RA patients compared with osteoarthritis controls (38). Thus, more research is necessary to determine if inflammatory arthritis is associated with a systemic marrow disorder and increased myelopoiesis.

The development of methods to distinguish “normal” red marrow from “pathologic” red marrow is of paramount importance. By combining 2 quantitative outcome measures of BME (Figure 6), we provide evidence that an objective prognostic threshold may exist. Interestingly, K/BxN mice with inflammatory arthritis (39) and constitutively active parathyroid hormone receptor-transgenic mice with noninflammatory hematopoiesis (40) also fit this model (data not shown). This threshold may be crossed when marrow vasculature is dysfunctional, leading to increased interstitial fluid in the tissue, as shown in Figure 5. Future studies with arthritis patients and healthy controls should be able to determine if a similar BME threshold also exists in humans.

ACKNOWLEDGMENTS

The authors would like to thank Patricia Weber for technical assistance with the MRI, Laura Yanoso for technical assistance with the micro-CT, Colleen Hock for assisting with animal breeding and genotyping, and Krista Scorsone for technical assistance with the histologic examinations.

Supported by research grants from Centocor and by grants from the US Department of Health and Human Services Public Health Service/NIH (AR-43510, AR-46545, AR-48697, AR-51469, AR-54041, DE-17096, and DK-64381).

REFERENCES

1. Feldmann M, Brennan FM, Maini RN. Rheumatoid arthritis. Cell 1996;85:307–10. [PubMed: 8616886]review
2. Firestein GS. Evolving concepts of rheumatoid arthritis. Nature 2003;423:356–61. [PubMed: 12748655]review
3. Feldmann M, Maini RN. TNF defined as a therapeutic target for rheumatoid arthritis and other autoimmune diseases. Nat Med 2003;9:1245–50. [PubMed: 14520364]published erratum appears in Nat Med 2003;9:1433
4. McQueen FM, Ostendorf B. What is MRI bone oedema in rheumatoid arthritis and why does it matter? Arthritis Res Ther 2006;8:222. [PubMed: 17169137]review
5. Appel H, Loddenkemper C, Grozdanovic Z, Ebhardt H, Dreimann M, Hempfing A, et al. Correlation of histopathological findings and magnetic resonance imaging in the spine of patients with ankylosing spondylitis. Arthritis Res Ther 2006;8:R143. [PubMed: 16925803]
6. Jimenez-Boj E, Nobauer-Huhmann I, Hanslik-Schnabel B, Dorotka R, Wanivenhaus AH, Kainberger F, et al. Bone erosions and bone marrow edema as defined by magnetic resonance imaging reflect true bone marrow inflammation in rheumatoid arthritis. Arthritis Rheum 2007;56:1118–24. [PubMed: 17393390]
7. McQueen FM. Magnetic resonance imaging in early inflammatory arthritis: what is its role? Rheumatology (Oxford) 2000;39:700–6. [PubMed: 10908686]review
8. McQueen FM, Benton N, Perry D, Crabbe J, Robinson E, Yeoman S, et al. Bone edema scored on magnetic resonance imaging scans of the dominant carpus at presentation predicts radiographic joint damage of the hands and feet six years later in patients with rheumatoid arthritis. Arthritis Rheum 2003;48:1814–27. [PubMed: 12847674]
9. Haavardsholm EA, Boyesen P, Ostergaard M, Schildvold A, Kvien TK. Magnetic resonance imaging findings in 84 patients with early rheumatoid arthritis: bone marrow oedema predicts erosive progression. Ann Rheum Dis 2008;67:794–800. [PubMed: 17981915]
10. McQueen FM, Stewart N, Crabbe J, Robinson E, Yeoman S, Tan PL, et al. Magnetic resonance imaging of the wrist in early rheumatoid arthritis reveals a high prevalence of erosions at four months after symptom onset. Ann Rheum Dis 1998;57:350–6. [PubMed: 9771209]

11. Kornaat PR, Bloem JL, Ceulemans RY, Riyazi N, Rosendaal FR, Nelissen RG, et al. Osteoarthritis of the knee: association between clinical features and MR imaging findings. Radiology 2006;239:811–7. [PubMed: 16714463]
12. Hofmann S, Kramer J, Vakil-Adli A, Aigner N, Breitenseher M. Painful bone marrow edema of the knee: differential diagnosis and therapeutic concepts. Orthop Clin North Am 2004;35:321–33. [PubMed: 15271540]reviewix
13. Braun J, Landewe R, Hermann KG, Han J, Yan S, Williamson P, et al. the ASSERT Study Group. Major reduction in spinal inflammation in patients with ankylosing spondylitis after treatment with infliximab: results of a multicenter, randomized, double-blind, placebo-controlled magnetic resonance imaging study. Arthritis Rheum 2006;54:1646–52. [PubMed: 16646033]
14. Van der Heijde D, Han C, DeVlam K, Burmester G, van den Bosch F, Williamson P, et al. Infliximab improves productivity and reduces workday loss in patients with ankylosing spondylitis: results from a randomized, placebo-controlled trial. Arthritis Rheum 2006;55:569–74. [PubMed: 16874778]
15. Jimenez-Boj E, Redlich K, Turk B, Hanslik-Schnabel B, Wanivenhaus A, Chott A, et al. Interaction between synovial inflammatory tissue and bone marrow in rheumatoid arthritis. J Immunol 2005;175:2579–88. [PubMed: 16081832]
16. Appel H, Kuhne M, Spiekermann S, Ebhardt H, Grozdanovic Z, Kohler D, et al. Immunohistologic analysis of zygapophyseal joints in patients with ankylosing spondylitis. Arthritis Rheum 2006;54:2845–51. [PubMed: 16947385]
17. Appel H, Kuhne M, Spiekermann S, Kohler D, Zacher J, Stein H, et al. Immunohistochemical analysis of hip arthritis in ankylosing spondylitis: evaluation of the bone-cartilage interface and subchondral bone marrow. Arthritis Rheum 2006;54:1805–13. [PubMed: 16736521]
18. Gortz B, Hayer S, Redlich K, Zwerina J, Tohidast-Akrad M, Tuerk B, et al. Arthritis induces lymphocytic bone marrow inflammation and endosteal bone formation. J Bone Miner Res 2004;19:990–8. [PubMed: 15125796]
19. Proulx ST, Kwok E, You Z, Beck CA, Shealy DJ, Ritchlin CT, et al. MRI and quantification of draining lymph node function in inflammatory arthritis. Ann N Y Acad Sci 2007;1117:106–23. [PubMed: 17646265]
20. Proulx ST, Kwok E, You Z, Papuga MO, Beck CA, Shealy DJ, et al. Longitudinal assessment of synovial, lymph node, and bone volumes in inflammatory arthritis in mice by in vivo magnetic resonance imaging and microfocal computed tomography. Arthritis Rheum 2007;56:4024–37. [PubMed: 18050199]
21. Li P, Schwarz EM, O'Keefe RJ, Ma L, Looney RJ, Ritchlin CT, et al. Systemic tumor necrosis factor α mediates an increase in peripheral CD11b^{high} osteoclast precursors in tumor necrosis factor α-transgenic mice. Arthritis Rheum 2004;50:265–76. [PubMed: 14730625]
22. Yao Z, Li P, Zhang Q, Schwarz EM, Keng P, Arbini A, et al. Tumor necrosis factor-α increases circulating osteoclast precursor numbers by promoting their proliferation and differentiation in the bone marrow through up-regulation of c-Fms expression. J Biol Chem 2006;281:11846–55. [PubMed: 16461346]
23. Kitaura H, Sands MS, Aya K, Zhou P, Hirayama T, Uthgenannt B, et al. Marrow stromal cells and osteoclast precursors differentially contribute to TNF-α-induced osteoclastogenesis in vivo. J Immunol 2004;173:4838–46. [PubMed: 15470024]
24. Kitaura H, Zhou P, Kim HJ, Novack DV, Ross FP, Teitelbaum SL. M-CSF mediates TNF-induced inflammatory osteolysis. J Clin Invest 2005;115:3418–27. [PubMed: 16294221]
25. Ritchlin CT, Haas-Smith SA, Li P, Hicks DG, Schwarz EM. Mechanisms of TNF-α- and RANKL-mediated osteoclastogenesis and bone resorption in psoriatic arthritis. J Clin Invest 2003;111:821–31. [PubMed: 12639988]
26. Keffer J, Probert L, Cazlaris H, Georgopoulos S, Kaslaris E, Kioussis D, et al. Transgenic mice expressing human tumour necrosis factor: a predictive genetic model of arthritis. EMBO J 1991;10:4025–31. [PubMed: 1721867]
27. Li P, Schwarz EM. The TNF-α transgenic mouse model of inflammatory arthritis. Springer Semin Immunopathol 2003;25:19–33. [PubMed: 12904889]review

28. Shealy DJ, Wooley PH, Emmell E, Volk A, Rosenberg A, Treacy G, et al. Anti-TNF-α antibody allows healing of joint damage in polyarthritic transgenic mice. Arthritis Res 2002;4:R7. [PubMed: 12223110]
29. Flick LM, Weaver JM, Ulrich-Vinther M, Abuzzahab F, Zhang X, Dougall WC, et al. Effects of receptor activator of NFκB (RANK) signaling blockade on fracture healing. J Orthop Res 2003;21:676–84. [PubMed: 12798068]
30. Franzoso G, Carlson L, Xing L, Poljak L, Shores EW, Brown KD, et al. Requirement for NF-κB in osteoclast and B-cell development. Genes Dev 1997;11:3482–96. [PubMed: 9407039]
31. Daldrup-Link HE, Henning T, Link TM. MR imaging of therapy-induced changes of bone marrow. Eur Radiol 2007;17:743–61. [PubMed: 17021706]review
32. Vogler JB III, Murphy WA. Bone marrow imaging. Radiology 1988;168:679–93. [PubMed: 3043546] review
33. Ostergaard M, Peterfy C, Conaghan P, McQueen F, Bird P, Ejbjerg B, et al. OMERACT rheumatoid arthritis magnetic resonance imaging studies: core set of MRI acquisitions, joint pathology definitions, and the OMERACT RA-MRI scoring system. J Rheumatol 2003;30:1385–6. [PubMed: 12784422][review] [published erratum appears in J Rheumatol 2004;31:198]
34. Hodgson R, Grainger A, O'Connor P, Barnes T, Connolly S, Moots R. Dynamic contrast enhanced MRI of bone marrow oedema in rheumatoid arthritis. Ann Rheum Dis 2008;67:270–2. [PubMed: 17965120]
35. Papadaki HA, Kritikos HD, Gemetzi C, Koutala H, Marsh JC, Boumpas DT, et al. Bone marrow progenitor cell reserve and function and stromal cell function are defective in rheumatoid arthritis: evidence for a tumor necrosis factor α-mediated effect. Blood 2002;99:1610–9. [PubMed: 11861275] published erratum appears in Blood 2007;109:4180
36. Tomita T, Shimaoka Y, Kashiwagi N, Hashimoto H, Kawamura S, Lee SB, et al. Enhanced expression of CD14 antigen on myeloid lineage cells derived from the bone marrow of patients with severe rheumatoid arthritis. J Rheumatol 1997;24:465–9. [PubMed: 9058650]
37. Tomita T, Takeuchi E, Toyosaki-Maeda T, Oku H, Kaneko M, Takano H, et al. Establishment of nurse-like stromal cells from bone marrow of patients with rheumatoid arthritis: indication of characteristic bone marrow microenvironment in patients with rheumatoid arthritis. Rheumatology (Oxford) 1999;38:854–63. [PubMed: 10515647]
38. Bugatti S, Caporali R, Manzo A, Vitolo B, Pitzalis C, Montecucco C. Involvement of subchondral bone marrow in rheumatoid arthritis: lymphoid neogenesis and in situ relationship to subchondral bone marrow osteoclast recruitment. Arthritis Rheum 2005;52:3448–59. [PubMed: 16258900]
39. Kouskoff V, Korganow AS, Duchatelle V, Degott C, Benoist C, Mathis D. Organ-specific disease provoked by systemic autoimmunity. Cell 1996;87:811–22. [PubMed: 8945509]
40. Calvi LM, Adams GB, Weibrecht KW, Weber JM, Olson DP, Knight MC, et al. Osteoblastic cells regulate the haematopoietic stem cell niche. Nature 2003;425:841–6. [PubMed: 14574413]

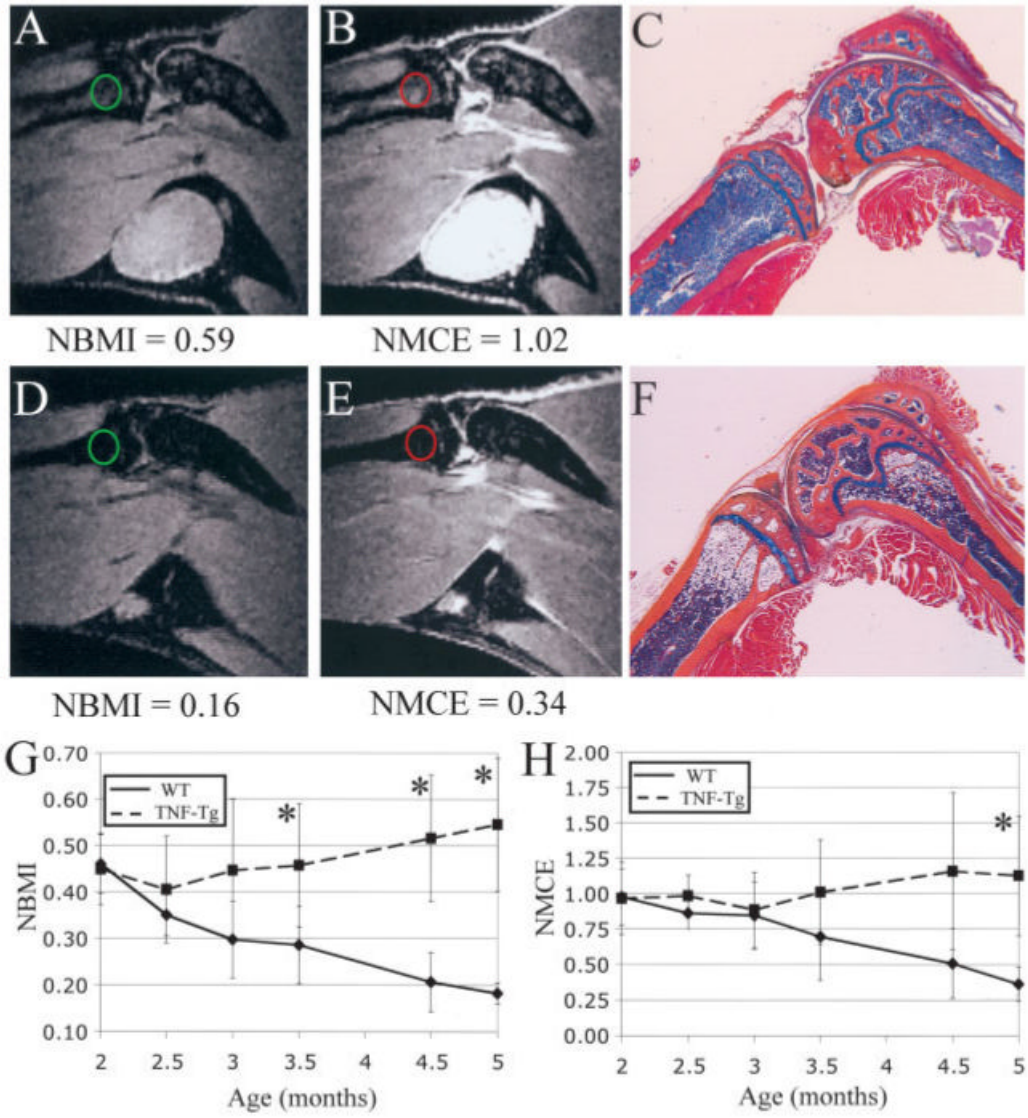

Figure 1.

Differences in the bone marrow of tumor necrosis factor-transgenic (TNF-Tg) and wild-type (WT) mice. **A-F,** Magnetic resonance images and corresponding orange G-Alcian blue-stained histologic sections of the knee joints from representative 5-month-old TNF-Tg mice (**A-C**) and WT mice (**D-F**). Features of the mice have been described previously (20). Quantification of bone marrow edema showed that marrow from TNF-Tg mice was hyperintense on precontrast images (**A**) (**circle**), and was brighter after contrast enhancement (**B**) (**circle**); these findings correlated with high cellularity throughout the marrow seen on histologic examination (**C**). In contrast, bone marrow of WT mice was hypointense (**D**) (**circle**), and showed little enhancement after injection of gadopentate dimeglumine (**E**) (**circle**). This low signal intensity correlated with a yellow marrow phenotype seen on histologic analysis (**F**). (Original magnification × 4.) **G** and **H,** Longitudinal measurement of normalized bone marrow intensity (NBMI) (**G**) and normalized marrow contrast enhancement (NMCE) (**H**) in 2-5-month-old WT and TNF-Tg mice. There was a highly significant decline in both NBMI and NMCE in WT mice. In comparison, TNF-Tg mice showed significant increases in both NBMI and NMCE. Values are the mean ± SD. * = $P < 0.05$ versus WT mice.

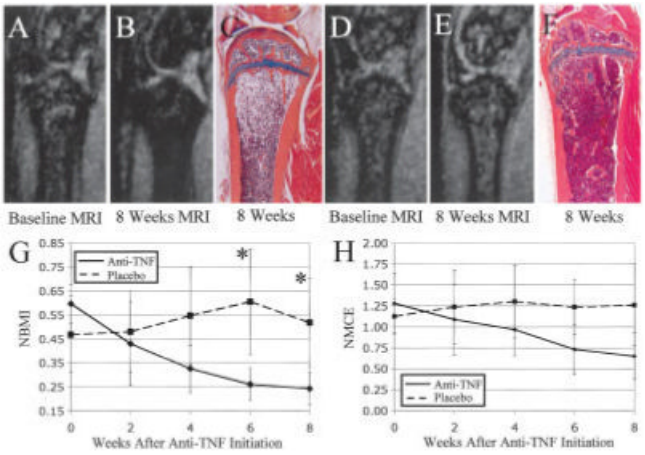

Figure 2.

Conversion of highly cellular marrow from TNF-Tg mice to yellow marrow with anti-TNF therapy. Magnetic resonance images (MRIs) of the proximal tibia were obtained at baseline (**A** and **D**) and 8 weeks after initiation of treatment (**B** and **E**) with anti-TNF (**A** and **B**) or placebo (**D** and **E**), as previously described (20). Anti-TNF therapy converted the highly cellular marrow to yellow marrow, as evidenced by hypointense marrow at 8 weeks (**B**) and highly fatty marrow in the corresponding histologic analysis performed after the mice were killed (**C**). Longitudinal quantification of the MRI signal in the marrow of these mice, using regression analysis, showed a highly significant decrease in NBMI (**G**) and NMCE (**H**) with therapy. In contrast, the marrow of placebo-treated mice remained hyperintense on MRI (**E**) and was highly cellular (**F**); quantification of the MRI signal in placebo-treated mice showed a significant increase in NBMI during the study (**G**). While significant differences in NBMI values were detected between the groups at 6 and 8 weeks (* = $P < 0.05$ versus WT mice), no significant differences in NMCE values were observed. Values in **G** and **H** are the mean ± SD. See Figure 1 for other definitions.

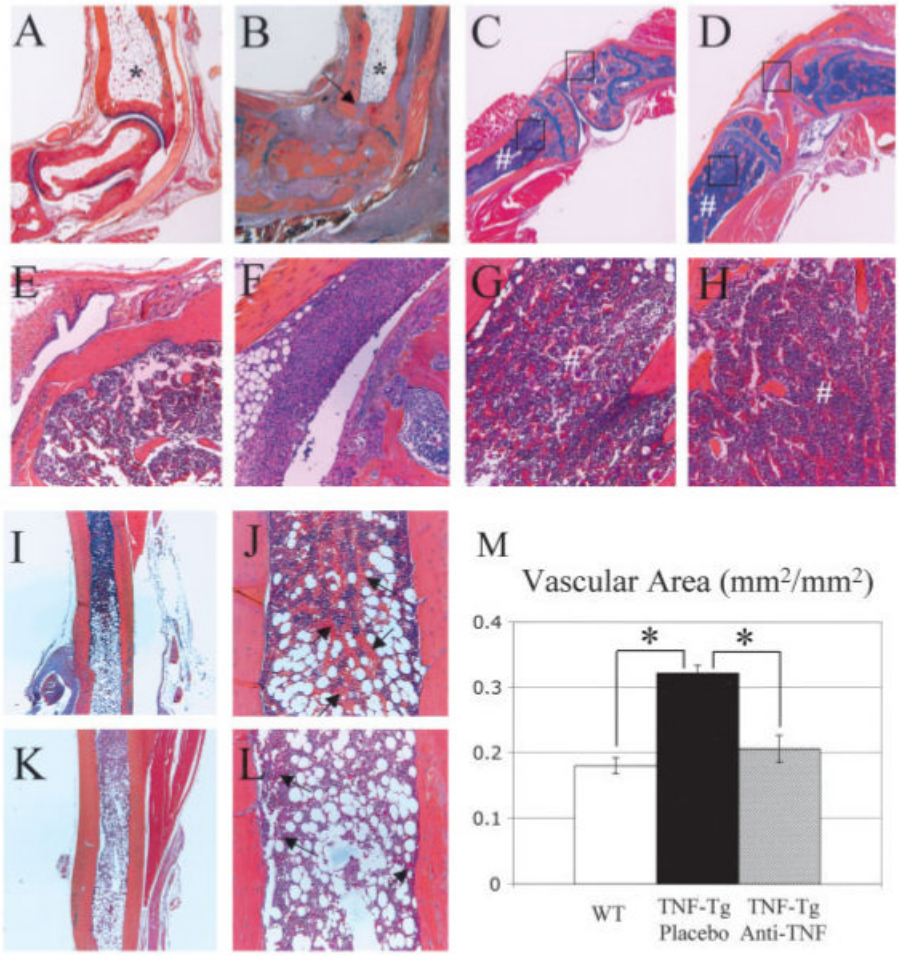

Figure 3.

Lack of red to yellow marrow conversion in TNF-Tg mice is caused by systemic effects rather than local joint inflammation and is reversed along a distal to proximal axis by anti-TNF therapy. **A-L,** Orange G-Alcian blue-stained histologic sections from representative 5-month-old WT and TNF-Tg mice. The marrow in the distal tibiae of both WT (**A**) and TNF-Tg (**B**) mice was equally filled with adipose tissue (*), despite the severe inflammation of the joint and focal bone erosion of the tibia (**arrow**). In contrast, the proximal tibiae of 2 representative 5-month-old TNF-Tg mice (**G** and **H**) were filled with red marrow (**#**), irrespective of the absence (**C** and **E**) or presence (**D** and **F**) of adjacent synovitis and focal erosions; boxed areas at the top of **C,** bottom of **C,** top of **D,** and bottom of **D** are shown at higher magnification in **E, G, F,** and **H,** respectively. Magnetic resonance imaging of this region (not shown) corroborated the finding of hyperintense marrow in the tibial metaphysis of both TNF-Tg mice. Histologic analysis of the distal tibial diaphyses of TNF-Tg mice without treatment (**I** and **J**) and after 8 weeks of anti-TNF therapy (**K** and **L**) highlighted the marrow conversion front. Note the highly vascular region at the yellow-red marrow interface in untreated mice, as evidenced by the large number of erythrocytes (**arrows** in **J**), in contrast with their paucity at this interface in anti-TNF-treated mice (**arrows** in **L**). **M,** Quantification of the vascular area in the red marrow of the midtibial diaphyses of WT, placebo-treated TNF-Tg, and anti-TNF-treated TNF-Tg mice (n = 3 per group), determined by histomorphometry of erythrocytic regions with point counting, as described in Materials and Methods. Values are the mean ± SD. * = $P < 0.01$. (Original magnification × 4 in **A-D, I,** and **K**; × 20 in **E-H, J,** and **L**.) See Figure 1 for definitions.

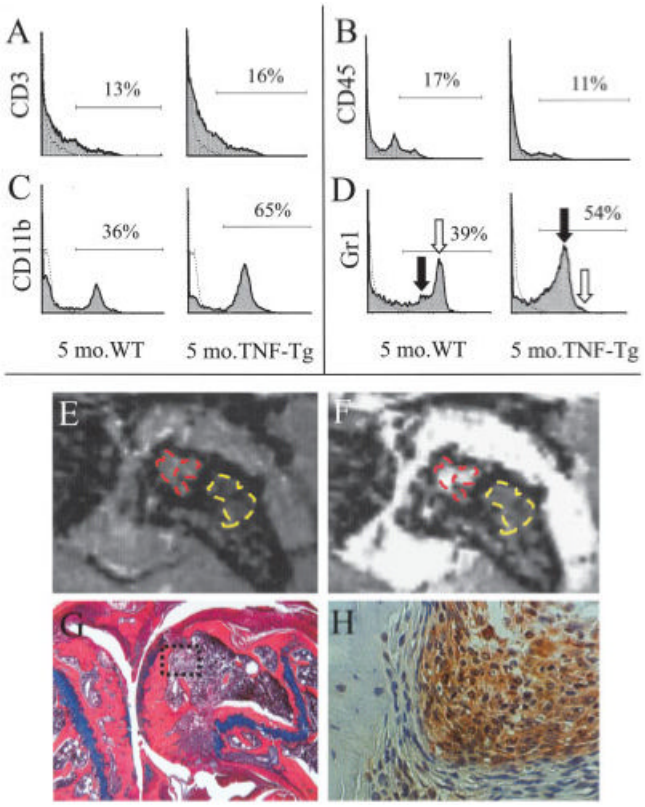

Figure 4.

Association of generalized bone marrow edema (BME) signals with increased myelopoiesis. **A-D,** Bone marrow cells harvested from 5-month-old WT and TNF-Tg mice were stained with labeled antibodies specific for CD3 (**A**), CD45 (**B**), CD11b (**C**), or Gr-1 (**D**), and analyzed by fluorescence-activated cell sorting. The histogram data from individual animals are representative of 3 independent experiments. Of note are the similar CD3+ and CD45+ cell frequencies in the marrow of WT and TNF-Tg mice, compared with the marked increase in the percentage of CD11b+ and Gr-1+ cells in TNF-Tg mice. Moreover, the increase in Gr-1+ cells is specifically in the Gr-1^{low} monocyte population (**solid arrow**), with a concomitant decrease in the Gr-1^{high} neutrophil population (**open arrow**). **E-H,** Magnetic resonance imaging (MRI) and histologic studies were performed in older (8-month-old) TNF-Tg mice with severe inflammatory erosive arthritis of the knee. Two distinct patterns of edema were seen, as evidenced by the representative findings shown. Precontrast MRIs (**E**) showed 2 hyperintense regions: subchondral (red) and in the femoral metaphysis (yellow). These regions were also apparent in the postcontrast image (**F**) (**E** and **F** are MRIs of the boxed area in **G**). In both cases, the mean signal intensity per pixel was markedly higher in the subchondral BME. The mouse was killed immediately after MRI scanning, and orange G-Alcian blue-stained histologic sections (**G**) revealed a cortical break in which synovial infiltrate from the pannus had penetrated into the subchondral marrow (original magnification × 10). Immunohistochemical analysis with antibodies specific for F4/80 revealed that the infiltrating cells adjacent to the subchondral osteoblasts were macrophages (**H**) (original magnification × 20). See Figure 1 for other definitions.

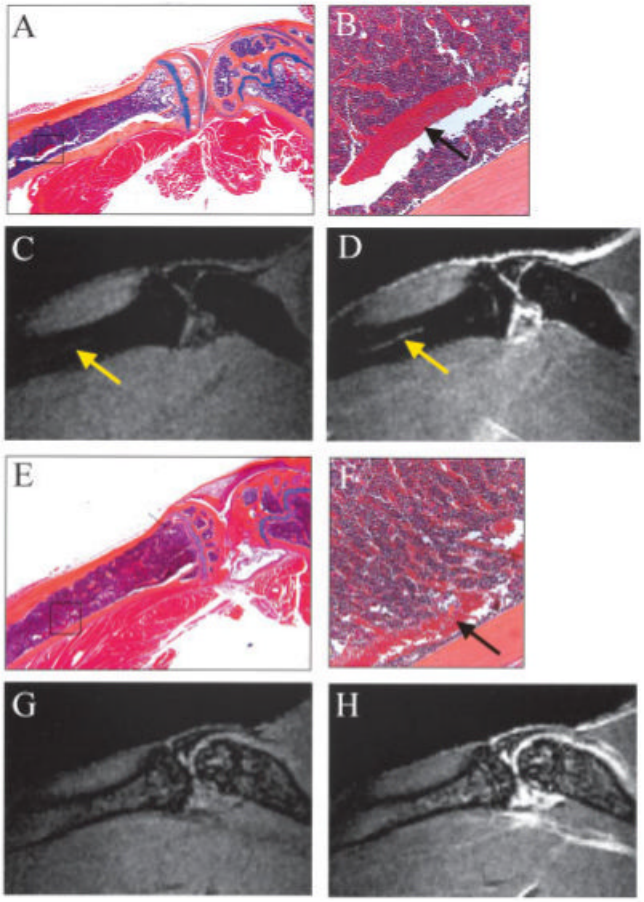

Figure 5.

Association of bone marrow edema in TNF-Tg mice with increased permeability of the blood-bone marrow barrier. **A** and **B,** Orange G-Alcian blue-stained histologic section from a 5-month-old WT mouse highlights the nutrient artery in the tibia (boxed area in **A** and **arrow** in **B**). Boxed area in **A** is shown at higher magnification in **B. C** and **D,** Precontrast (**C**) and postcontrast (**D**) magnetic resonance images (MRIs) of this tibia obtained immediately before the mouse was killed depict the nutrient artery as a bright line that is differentiated from hypointense red marrow (**arrows**). **E** and **F,** A similar histologic section from a 5-month-old TNF-Tg mouse shows the same red marrow phenotype adjacent to the nutrient artery (**arrow** in **F**) as was seen in the WT mouse. Boxed area in **E** is shown at higher magnification in **F. G** and **H,** Precontrast (**G**) and postcontrast (**H**) MRIs in the same animal show a hyperintense diffuse marrow pattern in which the nutrient artery can no longer be distinguished, indicating that there is no intact barrier between marrow vascularity and the bone marrow space. (Original magnification × 10 in **A**; × 40 in **E;** × 20 in **B** and **F.**) See Figure 1 for other definitions.

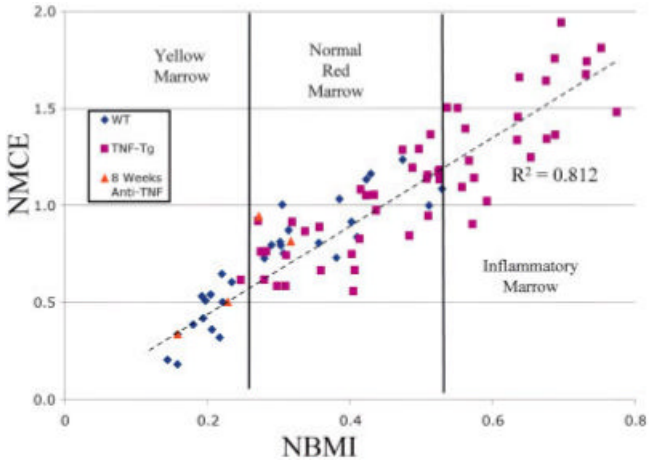

Figure 6.

Thresholds of yellow marrow, red marrow, and pathologic inflammatory bone marrow edema signals. Linear regression analysis of NBMI versus NMCE in the WT and TNF-Tg mice shown in Figure 1 and in anti-TNF-treated TNF-Tg mice after 8 weeks of therapy showed a highly significant association ($R^2 = 0.812$, $P < 0.0001$), using Pearson's correlation coefficient. Three groups of mice were differentiated in this plot. The first group was mice with yellow marrow and low values of both NBMI and NMCE. This group was composed exclusively of adult WT mice and 2 of the 4 anti-TNF-treated animals. The second group was mice with normal red marrow patterns and consisted of young WT mice, prearthritic TNF-Tg mice, and 2 of the 4 anti-TNF-treated mice. The third group contained only TNF-Tg mice with abnormal red marrow. See Figure 1 for definitions. Color figure can be viewed in the online issue, which is available at http://www.arthritisrheum.org.